# LennardJones bridge functions and triplet correlation functions

Phil Attard

Citation: The Journal of Chemical Physics **95**, 4471 (1991); doi: 10.1063/1.461770
View online: http://dx.doi.org/10.1063/1.461770
View Table of Contents: http://scitation.aip.org/content/aip/journal/jcp/95/6?ver=pdfcov
Published by the AIP Publishing

# Lennard-Jones bridge functions and triplet correlation functions

Phil Attard[a)]
*Department of Chemistry, University of British Columbia, Vancouver, British Columbia, Canada V6T 1Z1*

(Received 10 April 1991; accepted 7 June 1991)

Bridge functions and triplet potentials of mean force are calculated for the Lennard-Jones fluid using the binodal chain closure approximation. Inclusion of the former in the hypernetted-chain closure for the pair correlation functions leads to substantially improved values for the virial pressure. The triplet function also appears reliable, being in reasonable agreement with the solution to the spherically inhomogeneous Ornstein–Zernike equation.

## I. INTRODUCTION

Integral equation methods of classical equilibrium statistical mechanics are quantitatively accurate to a certain level of approximation for the two-particle correlation functions. There are two directions for further development of the theory: One might pursue systematic corrections to the two-particle approximation schemes, or one might seek to calculate three-particle functions. These two goals are not so disparate as they may at first appear, since the various two-body methods generally involve the truncation of some infinite expansion before the three-particle term. Hence there is a correspondence between corrections to two-particle closure approximations and expressions for the three-particle correlation functions. For example, the approximation embodied in the hypernetted-chain closure is the neglect of the bridge function, a function that to leading order involves an integral of the triplet direct correlation function. Therefore, an approximation for three-particle functions enables an improved quantitative treatment of the pair distribution function and of the consequent thermodynamic properties of the system.

This paper reports results for the bridge function and for the triplet distribution functions of the Lennard-Jones fluid. These are the first computations with the recently developed binodal chain (BNC) approximation scheme,[1] so-called because it approximates the bridge function by the binodal potential function, thereby systematically correcting the hypernetted-chain closure. This way of estimating the bridge function involves an iterative integral equation approach (in this respect it resembles the method of Verlet[2]); it is fundamentally more powerful than previous methods that relied on the quadrature of individual bridge diagrams.[3–8]

The binodal potential function is a convolution integral of certain three-particle functions, and these are approximated via a binodal-type closure to the triplet potential of mean force.[1] Previous approximation schemes for the three-particle functions include the Kirkwood superposition approximation,[9] equivalent to neglecting the triplet excess potential of mean force, the direct quadrature of individual three-particle diagrams,[10,11] and various more sophisticated approaches.[2,12–18] Of the schemes which apply some integral equation and closure approximation to the triplet potential of mean force, in terms of classes of diagrams it appears that Wertheim's[12] HNC II forms a subset of Attard's BNC,[1] which is itself a subset of Baxter's three-particle hypernetted chain (HNC).[13] Of further interest is Attard's source particle method,[18] which involves the solution of the spherically inhomogeneous Ornstein–Zernike equation, and which has been shown to be quite accurate for hard-sphere fluids.[19] Here, that method is applied to the Lennard-Jones fluid, and comparison is made with the BNC and with simulations.

This paper is divided into five main sections. Section II summarizes the equations that constitute the BNC approximation (Sec. II A), and discusses the computational (Sec. II B) and numerical (Sec. II C) aspects of the procedure. A triplet HNC approximation is derived in Sec. III, and its relation with other theories is discussed. Section IV describes the HNC3 source particle method,[18] outlining the equations (Sec. IV A) and the computational details (Sec. IV B). Numerical results for the BNC and the HNC3 approximations are given for a Lennard-Jones fluid, and comparison is made with simulations (Sec. V). A concluding section completes the paper (Sec. VI), except for an appendix on a fast Legendre transform.

## II. THE BNC APPROXIMATION

The equations which define the current implementation of the binodal chain (BNC) approximation are given in this section. Only the equations themselves are presented here since the full derivation has been given previously.[1] The computational algorithm and numerical details are also outlined.

### A. Analysis

A key quantity in the theory of triplet correlation functions is the three-particle negative excess potential of mean force $\tau(123)$, in terms of which the triplet distribution function is given by

$$g(123) = g(12)g(13)g(23)\exp\tau(123), \tag{2.1}$$

where $g(12)$ is the pair distribution function. The fundamental approximation in the binodal chain scheme is to truncate the representation of $\tau(123)$, summing only the mononodal and binodal functions

$$\tau(123) = \tau^{(1)}(1;23) + \tau^{(2)}(1;23). \tag{2.2}$$

The mononodal function is given by

$$\tau^{(1)}(1;23) = \int h(14)\eta(4;23)\rho(4)d4, \tag{2.3}$$

[a)] Present address: Department of Applied Mathematics, Research School of Physical Sciences, Australian National University, Canberra, Australian Capital Territory, Australia, 2601.

where $\rho(1)$ is the singlet density, $h(12)=g(12)-1$ is the total correlation function, and $\eta(1;23)$ is a particular ternary function. The binodal contribution to the potential is

$$\tau^{(2)}(1;23)=\eta(1;23)-\chi(1;23)-\tau^{(1)}(1;23)^2/2 - [\eta(\overline{1;2}3)-\chi(\overline{1;2}3)] - [\eta(\overline{1;3}2)-\chi(\overline{1;3}2)]. \quad (2.4)$$

The function $\chi(1;23)$ contains no binodal pairs of points, and $\eta(1;23)$ may be approximated by chains of $\chi(1;23)$,

$$\eta(1;23)=\chi(1;23)+\int\eta(1;24)\chi(4;23)\rho(4)d4 + \int\eta(1;34)\chi(4;23)\rho(4)d4. \quad (2.5)$$

The ternary functions $\eta(1;23)$ and $\chi(1;23)$ are analogous to the binary total and direct correlation functions, $h(12)$ and $c(12)$. In Eq. (2.4), the functions with overlined root points are the subsets of the full function with those root points connected directly by $h$ bonds. One has

$$\eta(\overline{1;2}3)=\chi(\overline{1;2}3)+\int\eta(\overline{1;2}4)\chi(4;23)\rho(4)d4. \quad (2.6)$$

Finally, two more equations complete a closed set,

$$\eta(1;23)=g(12)g(13)e^{\tau(123)}-h(12) - h(13)-1-\tau^{(1)}(1;23), \quad (2.7)$$

and

$$\eta(\overline{1;2}3)=h(12)g(13)e^{\tau(123)}-h(12). \quad (2.8)$$

These eight equations define the current implementation of the BNC approximation. It is worth emphasizing that even though Eqs. (2.3), (2.5), and (2.6) are approximate, the nature of the approximation is that certain diagrams in the Yvon-Mayer representation are neglected, and that no spurious diagrams are included.

The binodal chain approximation to the bridge function follows by truncating an expansion for the negative excess pair potential of mean force at the binodal term,

$$w(12)=w^{(1)}(12)+w^{(2)}(12). \quad (2.9)$$

The series or nodal function is

$$w^{(1)}(12)=\int c(13)h(32)\rho(3)d3. \quad (2.10)$$

The leading approximation to the bridge function is the binodal potential function,

$$w^{(2)}(12)=\tfrac{1}{2}\int\chi(1;34)\eta(2;34)g(34)\rho(3)\rho(4)d3\,d4 - \tfrac{1}{2}\int h(13)h(14)\eta^*(2;34)\rho(3)\rho(4)d3\,d4, \quad (2.11)$$

where

$$\eta^*(1;23)=h(12)h(13)+\int\eta(1;24)h(42)h(43)\rho(4)d4 + \int\eta(1;34)h(42)h(43)\rho(4)d4. \quad (2.12)$$

The triplet direct correlation function can also be calculated within the BNC approximation; it is given by

$$c(123)=g(23)\eta(1;23)-\eta^*(1;23). \quad (2.13)$$

For a given bridge function, the pair direct and total correlation functions are found from the Ornstein–Zernike equation,

$$h(12)=c(12)+\int c(13)h(32)\rho(3)d3, \quad (2.14)$$

and the closure relation

$$h(12)=\exp[-v(12)]-1, \quad (2.15)$$

where the potential of mean force is $v(12)=\beta u(12)-w(12)$, $\beta u(12)$ being the pair potential in units of the thermal energy, and $w(12)$, the negative excess potential of mean force, being given by Eq. (2.9).

### B. Computational

The algorithm to solve Eqs. (2.1)–(2.8) begins with three functions: $\eta(1;23)$, $\chi(1;23)$, and $\eta(\overline{1;2}3)$. These are from the last iterate, from a restart file, or from a first approximation which sets them each equal to $h(12)h(13)$. Each of these functions is Legendre transformed (see numerical details below), and the convolution integrals in Eqs. (2.3) and (2.6), and one of those in Eq. (2.5), are evaluated and stored. These three functions, the latter two being asymmetric in the minor root points, are then inverse Legendre transformed. The full symmetry of Eq. (2.5), and that of Eq. (2.4) using Eq. (2.6), is restored by adding the asymmetric function with swapped minor root points. At this stage one has $\beta(1;23)\equiv\eta(1;23)-\chi(1;23)$, and $\gamma(1;23)\equiv\beta(\overline{1;2}3)+\beta(\overline{1;3}2)$, as well as $\tau^{(1)}(1;23)$ from Eq. (2.3). Equation (2.4) is used to construct $\tau^{(2)}(1;23)$, and then a new value for $\eta(1;23)$ is obtained from Eq. (2.7). From this is subtacted $\beta(1;23)$ to give a new $\chi(1;23)$. Both these new functions are mixed with the old functions. Finally, $\eta(\overline{1;2}3)$ is found from Eq. (2.8), and the algorithm is repeated until satisfactory convergence is achieved.

For $\eta(1;23)$ and $\chi(1;23)$ given by the above procedure, one of the convolution integrals in Eq. (2.12) for $\eta^*(1;23)$ is evaluated by Legendre transformations of the functions comprising the integrand. The full $\eta^*(1;23)$ is constructed by adding the symmetric counterpart after Legendre inversion. In order to evaluate the convolution integral defining the binodal potential function, Eq. (2.11), it is necessary to first transform the functions comprising the integrand to a more symmetric grid before an appropriate Legendre and Hankel transformation (see numerical details below). An inverse Fourier transform yields $w^{(2)}(12)$.

A program which already solves the Ornstein–Zernike equation (using the standard method of fast Fourier transformation) for the HNC closure $[w^{(2)}(12)=0]$ is readily adapted to include the fixed binodal potential. This yields a new estimate of $h(12)$ which may be used to recalculate the ternary functions. The cycle of operations which comprise the preceding paragraphs is repeated until satisfactory convergence and self-consistency in all quantities is achieved.

### C. Numerical

The preceding discussion of the computational algorithm implicitly assumed procedures appropriate for a three-dimensional uniform simple fluid. Such a fluid has a constant density, pair correlation functions which depend solely upon the separation between the centers of the atoms, and triplet correlation functions depending only upon the triangle defined by the centers of three atoms. Equations (2.1)–(2.8) are most conveniently solved by representing the ternary functions by the two sides and cosine of the angle included at one of the minor root points, for example,

$$F(1;23) = F(r_{21},r_{23},x_{123}), \tag{2.16}$$

where $x_{123} = \mathbf{r}_{21}\cdot\mathbf{r}_{23}/r_{21}r_{23}$, and where $r = |\mathbf{r}|$. A typical convolution integral appearing in Eqs. (2.3), (2.5), or (2.6) becomes in this convention

$$F(r_{21},r_{23},x_{123}) = \rho\int G(r_{21},r_{24},x_{124})H(r_{24},r_{23},x_{423})\,d\mathbf{r}_4. \tag{2.17}$$

The discrete orthogonal Legendre transform pair of order $N$ is[18]

$$F(r_{21},r_{23},x_{123}) = \sum_{n=0}^{N-1}\hat{F}_n(r_{21},r_{23})P_n(x_{123}), \tag{2.18}$$

$$\hat{F}_n(r_{21},r_{23}) = \frac{2n+1}{2}\sum_{i=1}^{N} w_i F(r_{21},r_{23},x_i)P_n(x_i), \tag{2.19}$$

where $P_n(x)$ is the Legendre polynomial of order $n$, $x_i$ is the $i$th zero of $P_N(x)$, and $w_i$ are the weights associated with the Gauss–Legendre quadrature of order $N$. The convolution integral then partially factorizes, yielding[1]

$$\hat{F}_n(r_{21},r_{23}) = \frac{4\pi\rho}{2n+1}\int_0^\infty \hat{G}_n(r_{21},r_{24}) \times\hat{H}_n(r_{24},r_{23})r_{24}^2\,dr_{24}. \tag{2.20}$$

The one-dimensional convolution integral which remains is numerically tractable.

For the cases of Eq. (2.5), and Eq. (2.4) using Eq. (2.6), a symmetrized function must be formed. It is most efficient to estimate the second convolution integral by permuting the minor root points in the already calculated function. That is,

$$F_s(r_{21},r_{23},x_{123}) = F(r_{21},r_{23},x_{123}) + F(r_{31},r_{32},x_{132}), \tag{2.21}$$

where $r_{13}^2 = r_{12}^2 + r_{23}^2 - 2r_{12}r_{23}x_{123}$, and $x_{132} = (r_{23} - r_{12}x_{123})/r_{13}$. Trilinear interpolation was used to evaluate the function at the required nongrid points.

An important consideration in any three-particle computation is the amount of memory required. The algorithm discussed in the preceding section uses three permanent arrays [for the old values of $\eta(r_{21},r_{23},x_{123})$ and $\chi(r_{21},r_{23},x_{123})$, and for the Legendre transform of $h(r_{13})$ stored on the ternary grid] and four temporary arrays which are overwritten at various stages in the iteration cycle. Typical calculations (250 grid points for each of the two sides of the triangle, 40 angular nodes, single-precision 4 byte variables) required about 70 Mbytes. The mesh size was $dr = 0.02$.

The calculation of $w^{(2)}(r_{12})$, Eq. (2.11), involves a binary convolution integral. In this case the most convenient representation of the ternary function is

$$F(1;23) = F(r_{23},r_{123},y_{123}), \tag{2.22}$$

where $\mathbf{r}_{23} = \mathbf{r}_3 - \mathbf{r}_2$ is the vector joining the minor root points, where $\mathbf{r}_{123} = -\mathbf{r}_1 + (\mathbf{r}_2 + \mathbf{r}_3)/2$ is the vector from the major root point to the midpoint between the minor root points, and where $y_{123} = \mathbf{r}_{123}\cdot\mathbf{r}_{23}/r_{123}r_{23}$ is the cosine of the angle between these two vectors. Because the ternary functions are invariant under interchange of the minor root points, $F(1;23) = F(1;32)$, one has $F(r_{23},r_{123},y_{123}) = F(r_{23},r_{123},-y_{123})$. Consequently, the odd terms in its Legendre expansion vanish.

The functions $\eta(r_{21},r_{23},x_{123})$ and $\chi(r_{21},r_{23},x_{123})$ are read into the program that calculates $w^{(2)}(r_{12})$, and $\eta^*(r_{21},r_{23},x_{123})$ is calculated from Eq. (2.12) after Legendre transformation, one-dimensional convolution, inversion, and symmetrization, as discussed above. These three functions, as well as the function $\chi^*(r_{21},r_{23},x_{123}) = h(r_{12})h(r_{13})$, are represented on the new grid (based at the midpoint between the minor root points) using trilinear interpolation from the standard grid (based at a minor root point). That is,

$$r_{12}^2 = r_{23}^2/4 + r_{123}^2 - r_{23}r_{123}y_{123},$$
$$x_{123} = (r_{23}/2 - r_{123}y_{123})/r_{12}.$$

The discrete Legendre transforms of the ternary functions are performed, followed by the Hankel transform,

$$\tilde{F}_n(r_{23},k) = \int_0^\infty \hat{F}_n(r_{23},r_{123})j_n(kr_{123})r_{123}^2\,dr_{123}, \tag{2.23}$$

where $j_n(x)$ is the spherical Bessel function of order $n$. This transform was evaluated directly using Simpson's rule; the Bessel functions were calculated using forward or backward recurrence as appropriate. This procedure, of order $M^2$ ($M$ is the number of grid points for a side of the triangle) was used rather than Blum's[20] hat transform method ($\mathcal{O}M\log M$) because difficulties were experienced with the latter for larger values of $n$. The Fourier transform of the binodal potential function is[1]

$$\bar{w}^{(2)}(k) = \sum_{n=0}^{\infty}\frac{\rho^2(4\pi)^3}{4n+2}\int_0^\infty [g(r)\tilde{\chi}_n(r,k)\tilde{\eta}_n(r,k) - \tilde{\chi}_n^*(r,k)\tilde{\eta}_n^*(r,k)]r^2\,dr, \tag{2.24}$$

and its inverse Fourier transform is

$$w^{(2)}(r) = \frac{1}{2\pi^2 r}\int_0^\infty \bar{w}^{(2)}(k)\sin kr\,k\,dk. \tag{2.25}$$

Similarly sized and spaced grids were used in both the midpoint and in the minor root point representation. Of the order of 100 cycles were required at high densities for convergence of the virial pressure to four figures. The initial cycles included 5–10 iterations of the ternary functions, but the majority only required one iteration. A mixing parameter of 0.1 was used for $h(r)$ and for the ternary functions.

## III. THE HNC II APPROXIMATION

At the two-particle level, the BNC approximation goes beyond the HNC approximation by including the binodal potential function in addition to the mononodal or series function. A similar situation exists at the three-particle level, and this section focuses on the nodal contribution to the triplet potential of mean force. This simplification of the BNC approximation may be regarded as *the* triplet HNC closure. It turns out that the result is equivalent to the HNC II approximation of Wertheim,[12] and so the relationship between that work and the BNC approach is clarified by the present analysis. Further, the more approximate method offers certain advantages that are discussed below.

The triplet total correlation function is the connected subset of $g(123)$

$$h(123) = g(12)g(23)g(31)e^{\tau(123)} - h(12) - h(23) - h(31) - 1. \tag{3.1}$$

Note that $\tau(123)$ consists of density field points and no articulation points, $h$ bonds and no articulation pairs of points, and the 1-root points are nonadjacent and do not form an articulation triple. The triplet direct correlation function, $c(123)$, is the sum of connected diagrams without nodal points (in the $h$-bond representation, a root point connected with a single bond hangs from a node). Consequently, there is a three-particle Ornstein–Zernike equation which constructs $h(123)$ from $c(123)$ by appending nodes in all possible ways; this is given in the first line of Fig. 1. This expression, which is rather lengthy when the integrals are written out, is suitable for numerical computations; more succinct expressions involving $\delta$ functions may be useful for formal analysis.[15,21]

Because $\tau(123)$ has no direct bond between any of the three root points, it is necessary to identify the subsets of the triplet total and direct correlation functions that do. The connected diagrams with a $h(23)$ bond are

$$h(1\,\overline{23}) = g(12)h(23)g(31)e^{\tau(123)} - h(23). \tag{3.2}$$

This function may also be given in terms of $c(1\,\overline{23})$, the connected diagrams without nodes and with a $h(23)$ bond, as is manifest in the second line of Fig. 1.

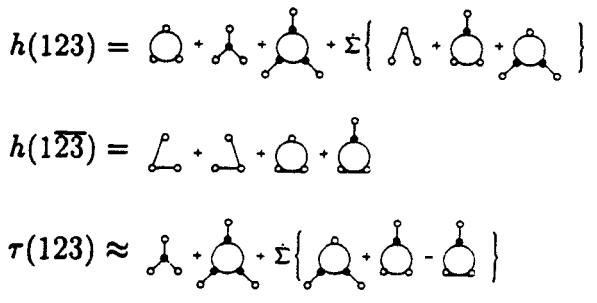

FIG. 1. The Ornstein–Zernike relation for $h(123)$ (first line), and for $h(1\,\overline{23})$ (second line), and the subset of $\tau(123)$ with nodal points (third line). The straight lines represent $h$ bonds, the solid circles are density field points, and the small open circles are 1-root points. The large circle is $c(123)$, and the subset with an $h(23)$ bond, $c(1\,\overline{23})$, has that bond shown explicitly. The operator $\hat{\Sigma}$ represents the sum of the three cyclic permutations of the root points.

The closure approximation represents the triplet negative excess potential of mean force by the nodal diagrams, as is shown explicitly in the last line of Fig. 1. The other two equations in that figure enable the closure to be rewritten,

$$\begin{aligned}\tau(123) = {} & h(123) - c(123) - [h(1\,\overline{23}) - c(1\,\overline{23})] \\ & - [h(2\,\overline{31}) - c(2\,\overline{31})] \\ & - [h(3\,\overline{12}) - c(3\,\overline{12})] \\ & + h(12)h(23) + h(23)h(31) + h(31)h(12).\end{aligned} \tag{3.3}$$

This forms a closed set of equations, since there are now five unknown functions, $h(123)$, $c(123)$, $h(1\,\overline{23})$, $c(1\,\overline{23})$, and $\tau(123)$, and five equations, (3.1), (3.2), (3.3), and the first two lines of Fig. 1, not counting the cyclic permutations. Wertheim's[12] original derivation of this result is more lengthy than that given here.

This mononodal HNC II method is more approximate than the BNC equations given in Sec. II. By this is meant that if $\eta(1;23)$ and $\chi(1;23)$ were exact, then Eqs. (2.3) and (2.5) would yield all the nodal diagrams generated by Eq. (3.3) [assuming $h(123)$ and $c(123)$ were exact] as well as an infinite set of diagrams not included in the latter. Although the precise nature of the approximations is obscured because the ternary functions are not exact, this conclusion still appears to hold, and one would expect the BNC approximation to be more accurate than the HNC II.

There is one advantage that the HNC II enjoys over the BNC, namely that it preserves the full symmetry of the ternary function. This is lost in the BNC approach because it distinguishes between major and minor root points. Baxter[13] also proposed a symmetric approximation scheme. He included all diagrams which could be written as single convolution integrals of ternary functions. In so far as all of the equations which currently comprise the BNC satisfy these criteria, one can see that the BNC diagrams form a subset of those included by Baxter. This would not be the case if the quaternary functions were retained in the BNC approximation.[1]

## IV. THE HNC3 APPROXIMATION

A source particle method for determining the triplet distribution function has been described by Attard.[18] Here, one considers an inhomogeneous fluid, with the inhomogeneity caused by an atom fixed at the origin. In this case the triplet distribution function of a uniform fluid is simply related to the inhomogeneous pair distribution function in the presence of the source particle. This section gives the equations that define that method as implemented here, including the computational algorithm and numerical details.

### A. Analysis

The source particle method for determining the triplet distribution function works for fluids that interact with spherically symmetric pair potentials, $u(12) = u(r_{12})$. The external potential representing the atom fixed at the origin is

$$V(1) = V(r_1) = u(r_1). \tag{4.1}$$

The singlet density of a spherically inhomogeneous fluid is a function of the distance from the origin, $\rho(1)=\rho(r_1)$, and the inhomogeneous pair correlation functions depend only upon the distances of the two particles from the origin and the cosine of their mutual angle, $h(12)=h(r_1,r_2,x_{12})$ and $c(12)=c(r_1,r_2,x_{12})$. The Legendre transform of the Ornstein–Zernike (OZ) equation for a spherically inhomogeneous fluid is[18,22]

$$\hat{h}_n(r_1,r_2)=\hat{c}_n(r_1,r_2)+\frac{4\pi}{2n+1}\int_0^\infty \hat{c}_n(r_1,r_3)\times\hat{h}_n(r_3,r_2)\rho(r_3)r_3^2\,dr_3. \tag{4.2}$$

Any of the various closures usually applied to uniform fluids may be used to relate the inhomogeneous pair correlation functions. For the present investigation, the hypernetted chain (HNC) was used,

$$h(r_1,r_2,x_{12})=-1+\exp[h(r_1,r_2,x_{12})-c(r_1,r_2,x_{12})-\beta u(r_{12})], \tag{4.3}$$

where $\beta=1/k_BT$ is the inverse temperature, and where $r_{12}^2=r_1^2+r_2^2-2r_1r_2x_{12}$.

There are three exact equations that relate the density profile to the external potential and the inhomogeneous pair correlation functions,[23–28] and, for the case of the HNC approximation, the coupling constant integration for the local chemical potential can be performed giving another equation for the profile.[29] In the present work the equation due to Treizenberg and Zwanzig[23] (TZ) was used. Its Legendre transform reads as[18]

$$\rho'(r_1)=-\beta\rho(r_1)V'(r_1)-\frac{4\pi\beta\rho(r_1)}{3}\times\int_0^\infty \hat{h}_1(r_1,r_2)V'(r_2)\rho(r_2)r_2^2\,dr_2, \tag{4.4}$$

where the prime denotes the derivative with respect to argument. [Note that a density is missing in Eq. (21) of Ref. 18.]

These equations are the HNC3 approximation, although perhaps a more illuminating appellation might be OZ-TZ-HNC. Note that because the profile is also solved to self-consistency, it is an approximation scheme for both the two- and three-particle distribution functions of the uniform fluid. These are given by

$$g(r_1)=\rho(r_1)/\rho \tag{4.5}$$

and

$$g(r_1,r_2,x_{12})=g(r_1)g(r_2)[1+h(r_1,r_2,x_{12})]. \tag{4.6}$$

The triplet negative excess potential of mean force is, within the HNC approximation,

$$\tau(r_1,r_2,x_{12})=h(r_1,r_2,x_{12})-c(r_1,r_2,x_{12})-[h^\infty(r_{12})-c^\infty(r_{12})], \tag{4.7}$$

where the superscipt denotes a bulk HNC pair correlation function.

### B. Computational and numerical considerations

The computational algorithm for the HNC3 approximation begins with the function

$$\hat{b}_n(r_1,r_2)=\hat{h}_n(r_1,r_2)-\hat{c}_n(r_1,r_2)$$

either from a restart file, from the last iterate, or from a first approximation which sets it equal to the bulk pair correlation functions calculated from the HNC closure for a uniform fluid. This is then inverse Legendre transformed, and the HNC closure, Eq. (4.3), is applied to form a new $h(r_1,r_2,x_{12})$. A new direct correlation function is then found from

$$c(r_1,r_2,x_{12})=h(r_1,r_2,x_{12})-b(r_1,r_2,x_{12}).$$

The Legendre transforms of both the total and the direct correlation functions are taken. A new density profile is formed by evaluating the right-hand side of Eq. (4.4), and this is mixed with the old density. [A first approximation for the density profile is simply the bulk HNC $\rho g(r)$.] A new $\hat{b}_n(r_1,r_2)$ is found from the Ornstein–Zernike equation (4.2), and this is also mixed with the previous estimate. The algorithm repeats until satisfactory convergence and self-consistency is obtained in the various thermodynamic properties.

All of the functions used in the computations are defined on some finite grid with cutoff $R$. Hence a correction ought be made for the truncation of the infinite integrals, Eqs. (4.2) and (4.4). The Ornstein–Zernike equation may be rewritten

$$\hat{b}_n(r_1,r_2)=\frac{4\pi}{2n+1}\int_0^R \hat{c}_n(r_1,r_3)\hat{h}_n(r_3,r_2)\times\rho(r_3)r_3^2\,dr_3+\hat{b}_n^\infty(r_1,r_2), \tag{4.8}$$

where the contribution from beyond the grid may be approximated by

$$\hat{b}_n^\infty(r_1,r_2)\approx\frac{4\pi\rho}{2n+1}\int_R^{2R}\hat{c}_n^\infty(r_1,r_3)\hat{h}_n^\infty(r_3,r_2)r_3^2\,dr_3. \tag{4.9}$$

In the above, the inhomogeneous pair correlation functions are only required on the grid, $r_1<R$, $r_2<R$. This last integrand consists of Legendre transforms of bulk HNC pair correlation functions. The density equation may be similarly corrected,

$$\rho'(r_1)=-\beta\rho(r_1)V'(r_1)-\frac{4\pi\beta\rho(r_1)}{3}\times\int_0^R\hat{h}_1(r_1,r_2)V'(r_2)\rho(r_2)r_2^2\,dr_2-\rho(r_1)\rho'_\infty(r_1), \tag{4.10}$$

where

$$\rho'_\infty(r_1)\approx\frac{4\pi\beta\rho}{3}\int_R^{2R}\hat{h}_1^\infty(r_1,r_2)V'(r_2)r_2^2\,dr_2. \tag{4.11}$$

The density itself follows by direct quadrature

$$\rho(r_1)=\int_R^{r_1}\rho'(r_2)dr_2+\rho(R), \tag{4.12}$$

with the boundary condition evaluated from the known asymptotic form of the pair distribution function[1,30]

$$\rho(R)\approx\rho[1-\kappa_T^2\beta u(R)]. \tag{4.13}$$

The isothermal compressibility was obtained by integrating the profile, with the tail correction determined by the

same asymptotic result

$$\kappa_T \approx 1 + 4\pi \int_0^R [\rho(r) - \rho] r^2 \, dr - 4\pi\rho\kappa_T^2 \beta u(R) R^3/3. \tag{4.14}$$

The appropriate root of this quadratic ensures that $\kappa_T \to 1$ as $\rho \to 0$. The internal energy per particle was taken to be

$$U/N \approx 2\pi \int_0^R u(r)\rho(r) r^2 \, dr + 2\pi\rho u(R) R^3/3, \tag{4.15}$$

and the compressibility factor followed from the virial pressure

$$\frac{\beta P}{\rho} \approx 1 - \frac{2\pi}{3} \int_0^R \beta u'(r)\rho(r) r^3 \, dr + 4\pi\rho\beta u(R) R^3/3. \tag{4.16}$$

These last three equations assume an $r^{-6}$ tail for the pair potential, but the procedure of correcting for the tail is obviously generally applicable. The sensitivity to the tail was checked by increasing $R$; the corrections discussed above gave more accurate results for a given cutoff than the simplest procedure that ignores all contributions from beyond the grid. The isothermal compressibility was the most difficult to obtain numerically, and the results at higher densities were not reliable. All integrals were evaluated using Simpson's rule.

The algorithm is such that three large arrays are required for the various inhomogeneous pair correlation functions, and one further array for the bulk correction, Eq. (4.9). Most of the single-precision calculations presented below used 300 mesh points in the radial directions, and 50 angular nodes, requiring about 40 Mbytes of memory. Note that because the Lennard-Jones potential is strongly repulsive at small separations, a hard-core cutoff of 0.7 was used. The radial grid spacing was 0.03, giving a large $R$ cutoff of 9.7. A mixing parameter of between 0.2 and 0.05 was used.

## V. RESULTS

Figures 2 and 3 show the internal energy per particle and the virial pressure as a function of density at $T^* = 2.74$. The dimensionless Lennard-Jones pair potential is

$$\beta u(r) = 4(r^{-12} - r^{-6})/T^*. \tag{5.1}$$

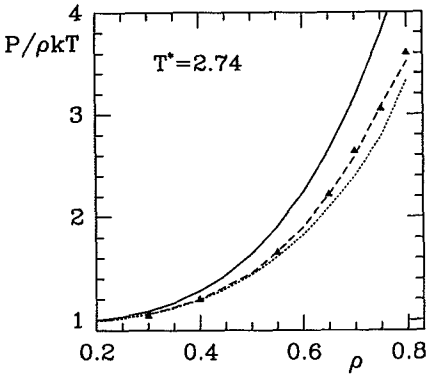


FIG. 3. Compressibility factor given by the HNC (solid curve), BNC (dashed curve), and HNC3 (dotted curve) approximations, and by simulations (Ref. 31).

The magnitude of the internal energy is increasingly underestimated by the HNC approximation, while both the BNC and the HNC3 are virtually coincident with the simulation data.[31] The virial pressure is significantly overestimated by the HNC at higher densities; the more sophisticated approximations are evidently much more reliable. The pressure is a very sensitive quantity which enables the BNC and the HNC3 to be distinguished. While the accuracy of the latter is quite acceptable, the agreement of the former with the simulation data is extraordinary. One can conclude that the binodal potential gives the dominant contribution to the bridge function, and that the BNC procedure itself is fundamentally sound.

The radial distribution function is compared to simulations[32] in Fig. 4 at the lower temperature of $T^* = 1.552$. The peak given by the BNC is slightly less than predicted by the HNC (the HNC3 would not be distinguishable from the BNC on this scale). The predicted compressibility factors are 0.70 (HNC), 0.55 (HNC3), 0.56 (BNC), to be compared to the simulation result 0.57.[33] Again one can see how sensitive a measure the virial pressure is, since the modifications to the radial distribution function are relatively minor. A $\tau^{(1)}$ approximation that consisted only of Eqs (2.3) and (2.7) was also briefly explored. This was in reasonable

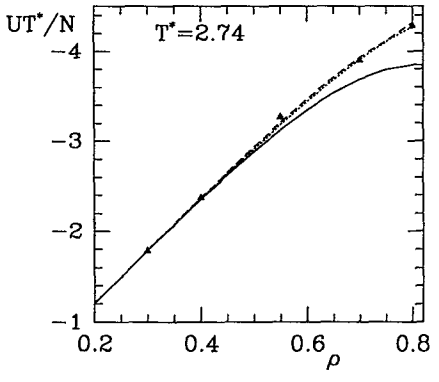


FIG. 2. Dimensionless internal energy per particle of a Lennard-Jones fluid given by the HNC (solid curve), BNC (dashed curve), and HNC3 (dotted curve) approximations, and by simulations (Ref. 31).

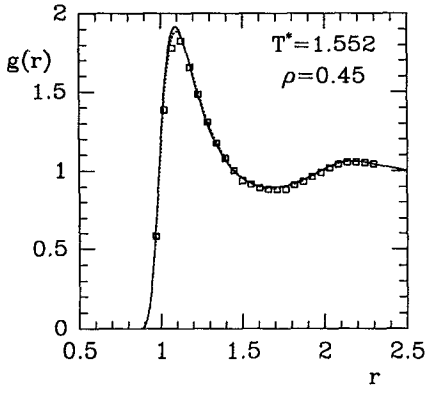


FIG. 4. Radial distribution function given by the HNC (solid curve), BNC (dashed curve), and HNC3 (dotted curve) approximations, and by simulations (Ref. 32).

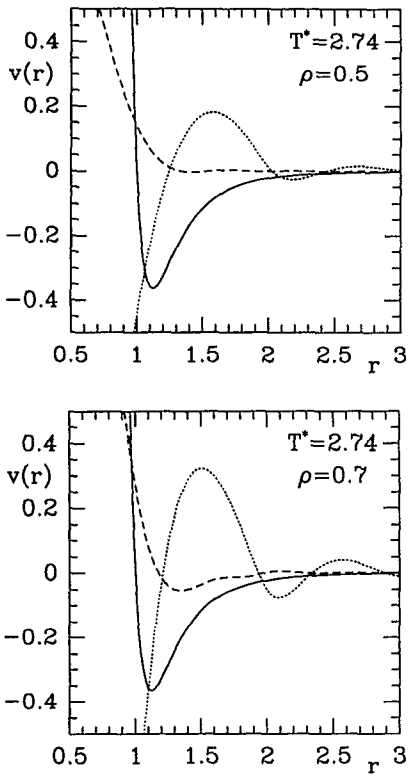


FIG. 5. Contributions to the potential of mean force (BNC approximation). The solid curve is the pair potential $\beta u(r)$, the dotted curve is the mononodal potential $-w^{(1)}(r) = c(r) - h(r)$, and the dashed curve is the binodal potential $-w^{(2)}(r)$.

agreement ($\rho/\delta kT = 0.56$) with the full BNC, which suggests that the HNC II approximation may be well-worth exploring.

The various contributions to the BNC potential of mean force, Eqs. (2.9) and (2.15), are given in Fig. 5. At small separations this is dominated by the repulsive part of the pair potential, Eq. (5.1). The contribution included by the HNC approximation, $w^{(1)}(r)$, is oscillatory in nature (period $\approx 1$), and it is evident that this gives the main indirect contribution to the potential of mean force. The region in which $w^{(2)}(r)$ does have a direct effect is around $r = 1$, and this is also where the virial pressure is most sensitive to small changes in $g(r)$. [Note that because of the self-consistent nature of the BNC, $w^{(2)}(r)$ contributes indirectly to $w^{(1)}(r)$. ] At the higher density of $\rho = 0.7$ [Fig. 5(b)], one sees that the structure in both $w^{(1)}(r)$ and $w^{(2)}(r)$ has increased.

The binodal potential function is the BNC approximation to the bridge function; its negative is plotted in Fig. 6 for various state points. In general, $-w^{(2)}(r)$ is positive in the region around $r = 1$, acting like an effective repulsion which lowers the peak of the HNC radial distribution function. On the other hand, the negative minimum evident around $r = 1.3$ increases the HNC prediction, which is itself approaching a minimum $r \approx 1.5$. In other words, the predominant effect of the highly connected bridge diagrams neglected by the HNC is to smooth the oscillations predicted by that theory. At fixed temperature, the magnitude of the bridge function increases as the density is increased. The effect of lowering the temperature is to increase the depth of the attractive well, and to lower the effective repulsion around

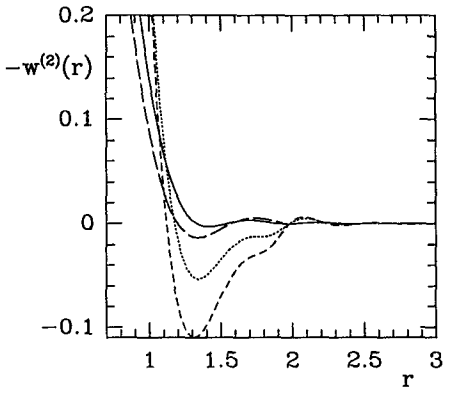


FIG. 6. The BNC approximation to the negative of the bridge function. The solid, dotted, and short-dashed curves are for $\rho = 0.5$, 0.7, and 0.75, at $T^* = 2.74$. The long-dashed curve is for $\rho = 0.45$, $T^* = 1.552$.

$r = 1$. Though the magnitude of the bridge function is small compared to $k_B T$, it obviously provides the subtle correction required by the HNC $g(r)$ (see Fig. 3). Compared to hard-sphere bridge functions (calculated from direct quadrature of bridge diagrams to order $\rho^3$),[8] these Lennard-Jones bridge functions exhibit a richer structure and are longer ranged.

The negative excess triplet potential of mean force is given in Fig. 7 for the particular configuration when all three particles are equidistant. There is agreement between the two approximate calculations and the simulations.[34] The latter were derived using

$$\tau(r,s,t) = \ln[g(r,s,t)/g(r)g(s)g(t)],$$

the argument of the logarithm being the published quantity.[34] The departure of $\tau(r,s,t)$ from zero measures the correction to the Kirkwood superposition aproximation; a positive value means that the triplet is more probable than is predicted by the latter approximation, and a negative value indicates that such triples occur less frequently than predicted by that classic ansatz. The HNC3 approximation quantitatively agrees with the simulations to within the statistical noise along the whole curve, whereas the BNC shows some systematic error for triangles with sides smaller than $r \approx 1.6$. Errors in $\tau(r,r,r)$ for $r < 0.9$ have negligible effect on $g(r,r,r)$ because $g(r) \approx 0$ in this region. Both approximations appear

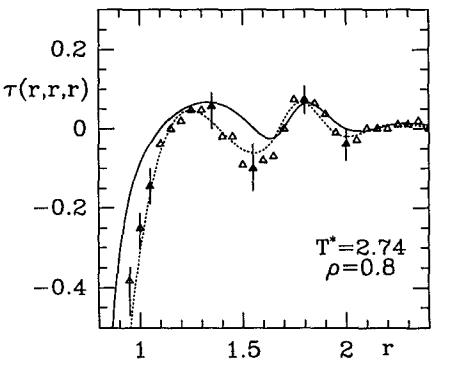


FIG. 7. The negative excess triplet potential of mean force, for equilateral triangle configurations given by the BNC (solid line) and by the HNC3 (dotted line), compared to data derived from simulations (Ref. 34).

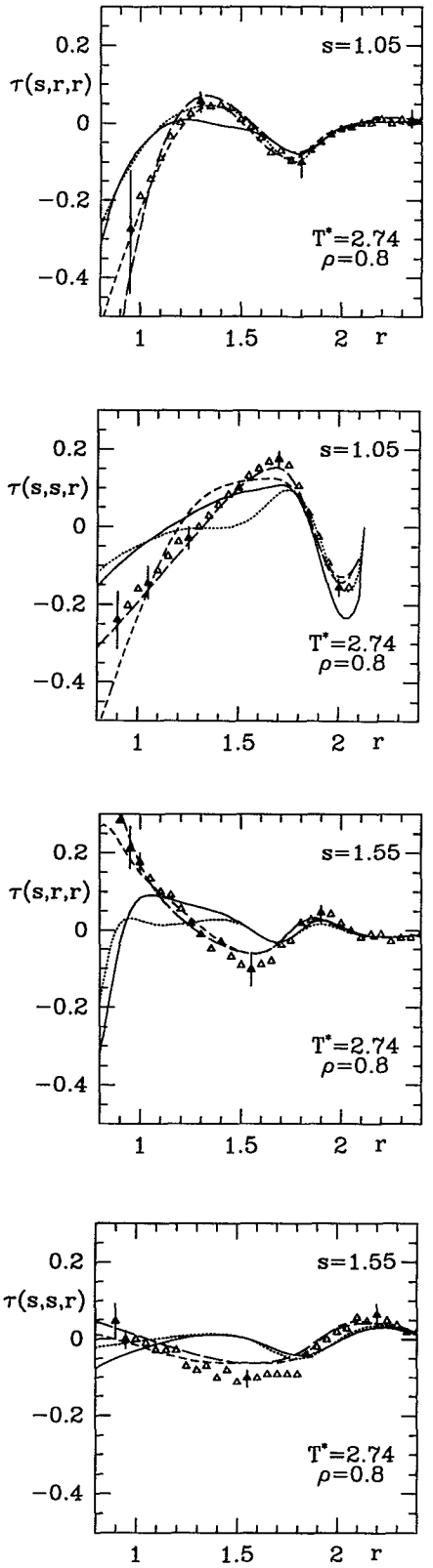


FIG. 8. The negative excess triplet potential of mean force, for isosceles triangle configurations, compared to data derived from simulations (Ref. 34). The solid line and the dotted line are the BNC approximation, and the short-dashed line and the long-dashed line are the HNC3 approximation. Both approximations distinguish one of the three particles; the solid and the short-dashed curves are when the distinguished particle corresponds to the unique vertex of the isosceles triangle, and the dotted and the long-dashed curves are when it represents one of the two equivalent vertices.

slightly better than the theory of Haymet, Rice, and Madden,[11] which evaluates the first eight triplet $h$-bond diagrams, although that direct approach is not bad at this temperature.[34]

Figure 8 shows the negative excess triplet potential of mean force for isosceles triangle geometry. Because neither the BNC nor the HNC3 preserves the full symmetry of the exact function, the particle distinguished by the approximations may be assigned to one of two distinct vertices of the isosceles triangle, giving the two curves for each approximation in each figure. In a fully symmetric theory the members of each pair would be coincident. Broadly speaking, the departure from full symmetry is about the same order as the error of the approximation itself. Hence even in the absence of simulation data, one could estimate the error of the approximate theory. The HNC3 theory is almost everywhere within the statistical noise of the simulations, whereas the BNC tends to show systematic departures for small $r$. It's worth mentioning that the lower density and temperature state point $\rho = 0.45$, $T^* = 1.552$ was also compared to simulations.[32] Qualitatively similar conclusions to the above were drawn, but in this case the noise in the simulation data prohibited a quantitative comparison.

Recently, Fushiki[35] used the source particle method[18] to calculate the triplet distribution function of a Lennard-Jones fluid at the state point $\rho = 0.85$, $T^* = 0.73$. The main difference with the present HNC3 calculations is that mainly the ZH closure was chosen, and that a fixed profile (i.e., not self-consistent) was used. Nevertheless, quite reasonable agreement was obtained with simulations at this more demanding temperature.

Figure 9 allows one an overall perspective of the behavior of $\tau(r,s,t)$ at the state point $\rho = 0.5$, $T^* = 2.74$. The magnitude of the function decreases as the particles are moved further apart, indicating that the Kirkwood superposition approximation dominates asymptotically. Further, the function is highly oscillatory, and the sign of the central peak appears to change regularly (with period $r = 1$) as the two fixed atoms are separated. The exact triplet function would have two mirror planes on this plot, at $y = 0$ and at $x = r/2$. Once again one can see that the departure of the BNC approximation from full symmetry is relatively small.

It is possible to gain insight into the behavior of $\tau(r,s,t)$ by considering the errors in the Kirkwood superposition approximation (KSA). The KSA takes the probability of a triplet to be the product of the pair probabilities, and $\tau(r,s,t)$ measures the departure from this independent probability assumption due to the presence of a third particle. When the third particle is far removed from the remaining pair, it can have no influence on them, and the KSA is exact, with $\tau(r,s,t) \to 0$. This is confirmed by Figs. 7–9. The maxima in the pair distribution function $g(r)$ are essentially due to the favorable packing of solvent between the pair, or, in the case of contact ($r \approx 1$), the buildup of solvent around the pair. A third particle fixed nearby can be expected to disturb these favorable configurations. Hence one would anticipate that the KSA generally overestimates the peaks in $g(r,s,t)$, and $\tau(r,s,t)$ should be negative here. On the other hand, the minima in $g(r)$ arise from solvent exclusion between the two

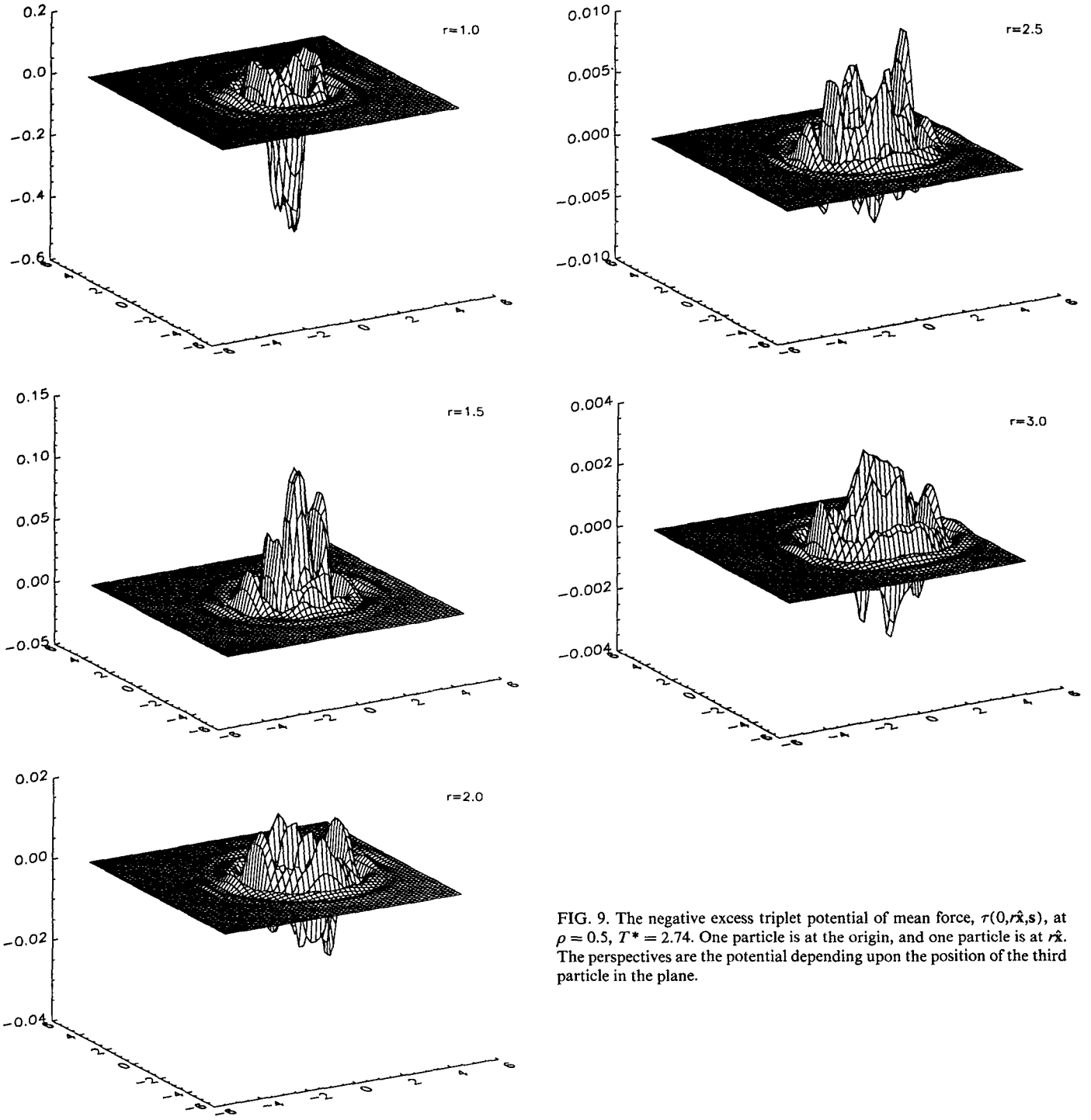


FIG. 9. The negative excess triplet potential of mean force, $\tau(0,r\hat{\mathbf{x}},\mathbf{s})$, at $\rho = 0.5$, $T^* = 2.74$. One particle is at the origin, and one particle is at $r\hat{\mathbf{x}}$. The perspectives are the potential depending upon the position of the third particle in the plane.

particles due to unfavorable packing. The depleted region between the pairs of particles in a triple is shared between them, suggesting that the KSA will generally overestimate the depth of the minima in $g(r,s,t)$, and $\tau(r,s,t)$ should be positive here. In summary, the highly connected diagrams comprising $\tau(r,s,t)$ neglected by the KSA tend to damp the oscillations it predicts for $g(r,s,t)$. Note the similarity of this argument with the discussion of the effects of the bridge function on the HNC $g(r)$.

These general observations are consistent with the present computations. $\tau(r,r,r)$ is negative in Fig. 7 for $r \approx 1$, 2, and the potentials in Fig. 8 are mostly negative for $s = 1.05$ and mostly positive for $s = 1.55$. Similarly, in Fig. 9 the potential on average has a sign determined by whether $r$ is integer or half-integer, corresponding to maxima or minima in $g(r)$. [Figures 8 and 9 can only be discussed "on average" because only one or two of the triple are held fixed near a maximum or a minimum of $g(r)$.] The behavior of $\tau(r,s,t)$ discussed above holds only in general, and more detailed arguments may be required for specific cases. For example, $\tau(r,r,r)$ is negative for $r \approx 1.5$, apparently due to the third particle preventing the favorable buildup of fluid at the

boundary of the cavity between a pair; in this case the configuration is even more unlikely than is predicted by the KSA.

## VI. CONCLUSION

This paper has been mainly concerned with establishing the BNC approximation, and with obtaining specific results for the bridge function and for the triplet distribution function of the Lennard-Jones fluid. The first goal may be considered achieved since it was shown that the BNC returned virtually exact results for the virial pressure, at least along the isotherm $T^* = 2.74$. From this one may also conclude that the binodal potential is the dominant contribution to the bridge function, and that the BNC approximation gives this quantity with high accuracy. As far as the triplet distribution function was concerned, both the BNC and the HNC3 approximations were in reasonable agreement with simulations. In contrast to the pair case, the source particle approach appeared the more accurate of the two for the triplet function, perhaps suggesting that there is room for further development of the BNC theory at the triplet level.

Several directions for future research are indicated by the present investigation. Because of the superiority of the BNC and the source particle approach over conventional closures, a more complete survey of the Lennard-Jones fluid may be appropriate, particularly near the critical point and the coexistence line. Beyond this the approaches may be applied to other fluids where not much is known about either the bridge function or the three-particle distribution function. Finally, these two relatively sophisticated theories may both stimulate and test simpler approaches. One wonders whether a recent improvement upon the Kirkwood superposition approximation for hard spheres in rolling contact[19] may be applicable to other fluids or other configurations.

## ACKNOWLEDGMENTS

The financial support of the Natural Sciences and Engineering Council of Canada and of the Killam Foundation at the University of British Columbia is gratefully acknowleged.

## APPENDIX: QUICK LEGENDRE TRANSFORM

The expansion of a function in Legendre polynomials frequently occurs in numerical applications. The orthogonal discretization[1] is convenient for computational work because it supresses the buildup of round-off error, and because there is no redundancy in the information contained in the two representations of the function in angular and in Legendre space. Since the forward and inverse transforms can occupy a substantial portion of the computational algorithms discussed in the text, it seems worthwhile to inquire of the possibility of a fast Legendre transform.

The discrete orthogonal Legendre transform of order $N$ is[1]

$$\hat{f}_n = \sum_{i=1}^{N} W_{n,i} f_i, \quad f_i = \sum_{n=0}^{N-1} P_n(x_i)\hat{f}_n, \tag{A1}$$

where $x_i$ is the $i$th node of the Legendre polynomial of order $N$, $P_N(x_i) = 0$, and where

$$W_{n,i} = \frac{2n+1}{1-x_i^2}\frac{P_n(x_i)}{P'_N(x_i)^2}. \tag{A2}$$

Now $x_{N-i+1} = -x_i$, and $W_{n,N-i+1} = (-1)^n W_{n,i}$. Assume $N$ is even, and define

$$f_i^{\pm} = f_i \pm f_{N-i+1}, \quad 1 \leqslant i \leqslant N/2. \tag{A3}$$

Then,

$$\hat{f}_{2n} = \sum_{i=1}^{N/2} W_{n,i} f_i^{+}, \quad \hat{f}_{2n+1} = \sum_{i=1}^{N/2} W_{n,i} f_i^{-}, \quad 0 \leqslant n \leqslant N/2, \tag{A4}$$

and

$$f_i^{+} = 2\sum_{n=0}^{N/2-1} P_{2n}(x_i)\hat{f}_{2n},$$
$$f_i^{-} = 2\sum_{n=0}^{N/2-1} P_{2n+1}(x_i)\hat{f}_{2n+1}, \quad 1 \leqslant i \leqslant N/2, \tag{A5}$$

from which the original $f_i$ are easily recovered using Eq. (A3). These equations represent two forward and two inverse transforms, each of order $N/2$. This halves the number of multiplications required by the original formulation, Eq. (A1). Even though the transform is not truly "fast," this savings is still valuable.

[1] P. Attard, J. Chem. Phys. **93**, 7301 (1990); erratum **94**, 6936 (1991).
[2] L. Verlet, Physica **30**, 95 (1964); **31**, 959 (1965).
[3] B. R. A. Nijboer and L. van Hove, Phys. Rev. **85**, 777 (1952).
[4] H. Iyetomi and S. Ichimaru, Phys. Rev. A **27**, 3241 (1983).
[5] R. Bacquet and P. Rossky, J. Chem. Phys. **79**, 1419 (1983).
[6] L. Ballone, G. Pastore, and M. P. Tosi, J. Chem. Phys. **85**, 2943 (1986).
[7] J. Wiechen, J. Chem. Phys. **85**, 7364 (1986).
[8] P. Attard and G. N. Patey, J. Chem. Phys. **92**, 4970 (1990).
[9] J. G. Kirkwood, J. Chem. Phys. **3**, 300 (1935).
[10] S. A. Rice and J. Lekner, J. Chem. Phys. **42**, 3559 (1965).
[11] A. D. J. Haymet, S. A. Rice, and W. G. Madden, J. Chem. Phys. **74**, 3033 (1981).
[12] M. S. Wertheim, J. Math. Phys. **8**, 927 (1967).
[13] R. J. Baxter, Ann. Phys. (N.Y.) **46**, 509 (1968).
[14] F. J. Pinski and C. E. Campbell, Phys. Rev. A **33**, 4232 (1986).
[15] J. L. Barrat, J. P. Hansen, and G. Pastore, Mol. Phys. **63**, 747 (1988).
[16] J. Blawzdziewicz, B. Cichocki, and R. Holyst, Physica A **157**, 857 (1989).
[17] J. Blawzdziewicz, B. Cichocki, and G. Szamel, J. Chem. Phys. **91**, 7467 (1989).
[18] P. Attard, J. Chem. Phys. **91**, 3072 (1989).
[19] P. Attard, Mol. Phys. (in press).
[20] L. Blum, J. Chem. Phys. **58**, 3295 (1973).
[21] J. R. Henderson, Phys. Rev. A **36**, 4527 (1987).
[22] M. Fushiki, Chem. Phys. Lett. **154**, 77 (1989).
[23] D. G. Triezenberg and R. Zwanzig, Phys. Rev. Lett. **28**, 1183 (1972).
[24] R. A. Lovett, C. Y. Mou, and F. P. Buff, J. Chem. Phys. **58**, 1880 (1976).
[25] M. S. Wertheim, J. Chem. Phys. **65**, 2377 (1976).
[26] M. Born and H. S. Green, Proc. R. Soc. London Ser. A **188**, 10 (1946).
[27] J. Yvon, *La Théorie Statistique des Fluides et L'Equation d'État*, Actualités Scientifiques et Industrielles, Vol. 203 (Hermann, Paris, 1935).
[28] N. N. Bogoliubov, J. Phys. (Moscow) **10**, 256 (1946).
[29] R. Kjellander and S. Marčelja, J. Chem. Phys. **82**, 2122 (1985).
[30] G. Stell, *Statistical Mechanics. Part A: Equilibrium Techniques*, edited by Bruce J. Berne (Plenum, New York, 1977).
[31] L. Verlet and D. Levesque, Physica **36**, 254 (1967); D. Levesque and L. Verlet, Phys. Rev. **182**, 307 (1969).
[32] J. A. Krumhansl and S-s. Wang, J. Chem. Phys. **56**, 2034 (1972).
[33] L. Verlet, Phys. Rev. **159**, 98 (1967).
[34] W. J. McNeil, W. G. Madden, A. D. J. Haymet, and S. A. Rice, J. Chem. Phys. **78**, 388 (1983).
[35] M. Fushiki, Mol. Phys. (submitted).